




Received January 20, 2021; revised February 25, 2021; accepted March 6, 2021; date of publication March 10, 2021; date of current version April 28, 2021.

Digital Object Identifier 10.1109/TQE.2021.3065227

# Rydberg Atom Electric Field Sensors for Communications and Sensing

CHARLES T. FANCHER<sup>1</sup> , DAVID R. SCHERER<sup>2</sup>  (Senior Member, IEEE),  
MARC C. ST. JOHN<sup>1</sup> (Member, IEEE),  
AND BONNIE L. SCHMITTBERGER MARLOW<sup>1</sup> 

<sup>1</sup>Emerging Engineering and Physical Sciences Department, The MITRE Corporation, McLean, VA 22102 USA

<sup>2</sup>The MITRE Corporation, Bedford, MA 01730 USA

Corresponding author: Charles T. Fancher (e-mail: cfancher@mitre.org)

**ABSTRACT** Rydberg atom electric field sensors are projected to enable novel capabilities for resilient communications and sensing. This quantum sensor is small-size, highly sensitive, and broadly tunable, and it has the potential for performing precision vector electric field and angle-of-arrival measurements. While these atomic electric field sensors will not replace traditional receivers in commodity applications for RF signal reception, these sensors could be an enabling technology in niche application spaces. This review outlines the principles of operation of atomic electric field sensors and compares their performance capabilities to traditional RF receivers. It also highlights recent research and development efforts in atomic electric field sensing and identifies applications for which these sensors are projected to impact communications and remote sensing.

**INDEX TERMS** Antenna, atomic sensors, communications technology, quantum sensing, receiver, remote sensing, Rydberg atoms.

## I. INTRODUCTION

Atomic electric field sensors are projected to enable novel capabilities for niche applications in communications and sensing, especially in situations where the carrier frequency is known. This emerging quantum technology has key performance advantages including good sensitivity, intrinsic accuracy, small physical size, narrow selectivity, and broad tunability [1]–[4]. In recent years, there has been a surge of new research and engineering of these sensors, including the development of a miniaturized sensor head [2], [5] and the first demonstration of angle-of-arrival measurements [6]. However, there is still substantial progress that must be made before this sensor can reach its full potential. This sensor could impact a range of applications for communications and sensing, including resistance to interference, electromagnetic spectrum situational awareness, and novel sensing capabilities.

The purpose of this review article is to provide an overview of the physics of atomic electric field sensors and recent research and development efforts as well as a novel perspective on sensor capabilities and potential application spaces. Specifically, the advantages and limitations as a function of carrier frequency are analyzed in Fig. 1, and the sensor performance is compared to traditional receivers (which

is defined here as including both antennas and front-end electronics) in terms of parameters including sensitivity, selectivity, and dynamic range.

Section II provides an overview of the physics of operation of atomic electric field sensors. Section III provides a comparison of the performance characteristics of atomic electric field sensors to traditional antennas and front-ends. Section IV describes the advantages of atomic electric field sensors, and Section V discusses their limitations. Section VI describes niche application spaces, which are projected to be impacted by further research and development of atomic electric field sensors.

## II. PRINCIPLE OF OPERATION

Traditional receivers and atomic electric field sensors have fundamentally different principles of operation. In Fig. 2, the schematic of an atomic electric field sensor is shown next to the analogous components in a generalized receiving antenna and front-end. In the atomic electric field sensor, lasers excite atoms to high-energy Rydberg states with a large principal quantum number  $n$  (where typically  $10 \leq n \leq 100$ ) in which the atoms act as highly sensitive electric dipoles. Incident RF/microwave radiation from near-DC to THz affects the internal state of Rydberg atoms, which in turn imposes

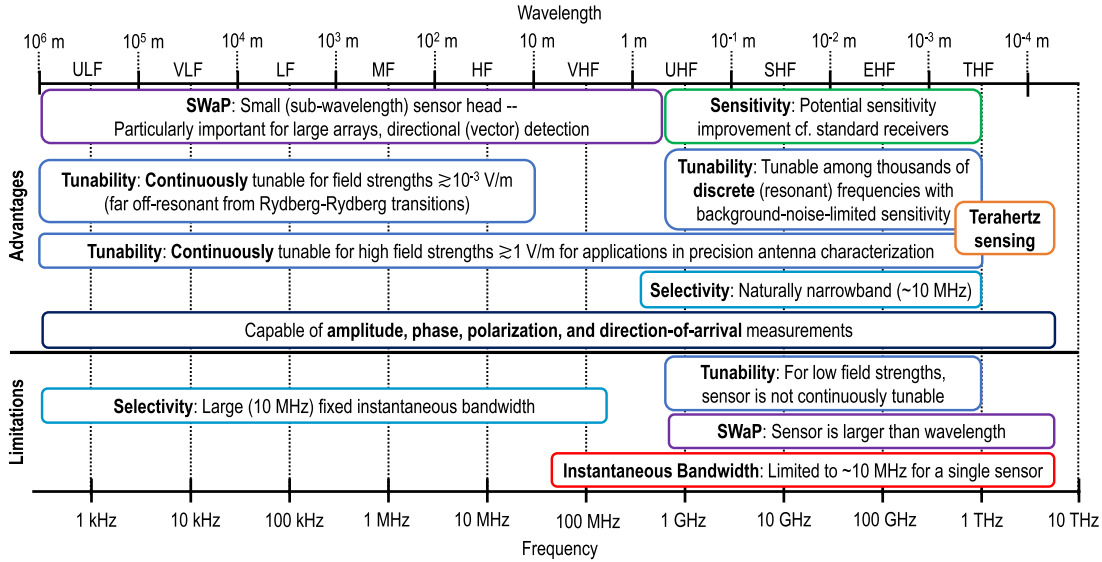


FIGURE 1. Advantages and limitations of atomic electric field sensors relative to traditional receivers as a function of carrier frequency (wavelength) at the bottom (top) on a logarithmic scale. The electromagnetic frequency bands are also shown. The acronym SWaP defines size, weight, and power.

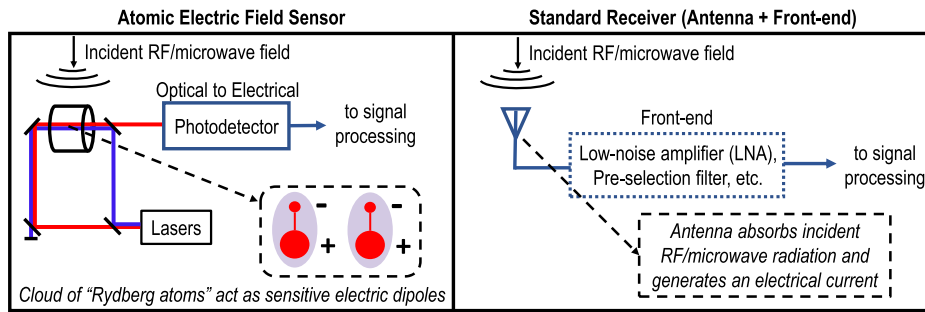


FIGURE 2. General schematic of the atomic electric field sensor versus a standard receiver for sensing incident RF or microwave radiation. The atomic electric field sensor and photodetector are analogous to the antenna and front-end electronics of a traditional receiver.

modulations on the optical fields passing through the atoms. These modulations are read out as spectral features on the electrical current produced by a photodetector. The coupling of incident RF or microwave radiation to the Rydberg atoms is a coherent process, which does not mandate any net absorption of the incoming radiation [7]. In contrast, traditional antennas operate by absorbing incident radiation, which drives free electrons and produces a current that carries the properties of the incident field. Section III provides more detailed comparisons between the atomic electric field sensor and two specific traditional receiver architectures (AM and heterodyne).

A typical schematic for exciting atoms to Rydberg states is shown in Fig. 3. Here, two optical fields counterpropagate through a glass cell filled with an atomic vapor. The probe optical field is used to excite the atom to a low-lying excited state, and the control optical field is used to excite the atom from the low excited state to a high-lying Rydberg state. In addition to this typical two-photon excitation scheme, there are also alternative three-photon excitation schemes that can be used to excite the atoms to Rydberg states [8]. Once in

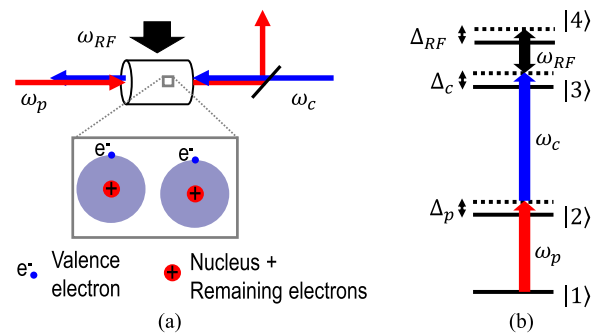


FIGURE 3. (a) An atomic electric field sensor typically employs two optical fields (frequencies  $\omega_p$  and  $\omega_c$ ) to excite atoms to highly excited states known as Rydberg states. The valence electron of a Rydberg atom is located far from the positively charged remainder of the atom, which creates a dipole that is highly sensitive to certain frequencies ( $\omega_{RF}$ ). (b) To excite rubidium (cesium) atoms to Rydberg states, one can apply a near-IR laser, typically with a wavelength of  $\lambda_p \approx 780$  nm ( $\lambda_p \approx 852$  nm), and a visible laser, typically with a wavelength of  $\lambda_c \approx 480$  nm ( $\lambda_c \approx 510$  nm). For the Autler-Townes detection technique, one operates with frequency detunings  $\Delta_c \approx 0$  (or  $\Delta_p \approx 0$ ) and  $\Delta_{RF} \approx 0$ , while  $\Delta_p$  ( $\Delta_c$ ) is either scanned across resonance or locked to a certain feature.

the Rydberg state ( $|3\rangle$ ), the atoms are highly sensitive to RF/microwave fields that are resonant or nearly resonant with transitions to nearby Rydberg states ( $|4\rangle$ ). If an incident RF/microwave field is far-off-resonant from a Rydberg–Rydberg transition, the field will still induce shifts in energy level  $|3\rangle$ . The properties of an incident RF/microwave field are measured via optical detection of the probe beam followed by spectral analysis.

There are two underlying physical phenomena that enable electric field measurements using Rydberg atoms: electromagnetically induced transparency (EIT) and AC Stark shifts, both of which arise due to the presence of electromagnetic fields with certain characteristics. Fig. 4 shows the consequence of each field on the transmission spectrum of the probe beam in an idealized case. In the case where only a probe optical field passes through the atoms, it undergoes strong absorption when its frequency is tuned close to resonance. This is shown in Fig. 4(a), where transmission through an optically thick vapor is shown. When the control field is turned ON and a fraction of atoms are excited to Rydberg states, one observes the phenomenon known as EIT, where a narrow window of high transmission is opened in the probe beam’s spectrum, as shown in Figs. 4(b) and (c). Finally, the presence of an RF/microwave field that is resonant or nearly resonant with a neighboring Rydberg state can induce Autler–Townes splitting, which is a version of an AC Stark shift in which the EIT transmission window splits, as depicted in Fig. 4(d). The Autler–Townes regime is the most sensitive operating regime of atomic electric field sensors owing to a resonant enhancement achievable when the incoming RF/microwave field is on or near resonance with certain atomic transitions. These resonances include thousands of discrete carrier frequencies between the ultra high frequency (UHF) and tremendously high frequency (THF) bands.

Off-resonant AC Stark shifts are used to measure fields with carrier frequencies below UHF. The off-resonant regime has poorer sensitivity than the resonant regime, but there have been proof-of-principle experiments indicating that this sensor can achieve continuous tunability down to near-DC for sufficiently strong electric fields [9]–[11].

The Autler–Townes splitting  $\Delta f_p$  observed in the spectrum of the probe beam is related to the strength of the RF/microwave field and the dipole moment of the transition by

$$\Delta f_p = \begin{cases} \frac{\lambda_c}{\lambda_p} \frac{\Omega_{RF}}{2\pi} & \text{if } \Delta_p \text{ is scanned} \\ \frac{\Omega_{RF}}{2\pi} & \text{if } \Delta_c \text{ is scanned} \end{cases} \quad (1a)$$

$$(1b)$$

where the ratio between the control and probe beam wavelengths ( $\lambda_c/\lambda_p$ ) accounts for the Doppler mismatch between the two fields [12], [13], and  $\Omega_{RF}$  is the Rabi frequency of the RF/microwave transition, given by

$$\Omega_{RF} = \frac{\vec{\mu}_{RF} \cdot \vec{E}_{RF}}{\hbar}. \quad (2)$$

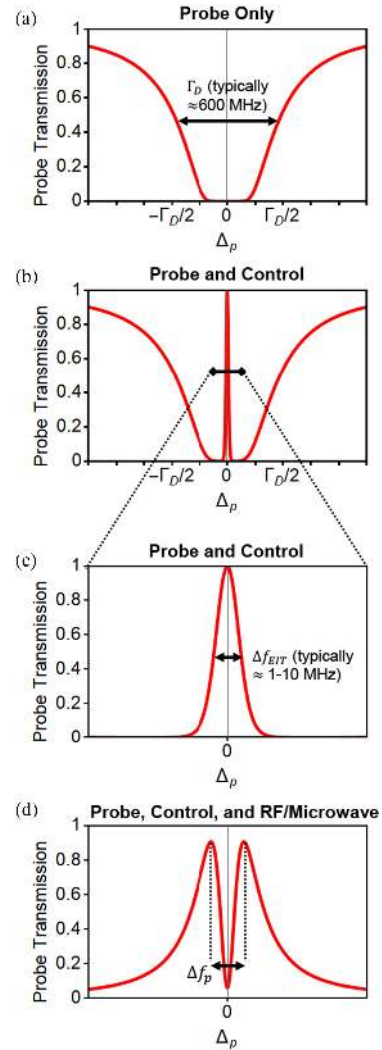


**FIGURE 4.** (a) Transmission dip of the probe beam tuned near resonance is characterized by the Doppler-broadened linewidth, which is a function of the temperature and density of the atoms. (Here, an optically thick vapor is shown, in which zero transmission is observed near resonance.) (b) Addition of the control beam induces a narrow transparency window (EIT). This is an idealized case; in practice, the transmission is unlikely to reach 100% due to Doppler broadening and other imperfections. (c) The same as (b), but showing a narrower frequency window. (d) Presence of an RF/microwave field that is resonant or nearly resonant with a nearby Rydberg state induces Autler–Townes splitting, where  $\Delta f_p$  is defined in (1b).

Here,  $\vec{\mu}_{RF}$  is the dipole moment of the transition,  $\vec{E}_{RF}$  is the amplitude of the RF/microwave field at the atoms, and  $\hbar$  is Planck’s constant divided by  $2\pi$ . The minimum resolvable frequency splitting  $\Delta f_p$  imposes a limit on the minimum detectable electric field amplitude  $E_{min}$ .

The minimum detectable electric field in the Autler–Townes regime was derived in [14] and is given by

$$E_{min} = \frac{h}{|\vec{\mu}_{RF}| T_{meas} \sqrt{N}} \quad (3)$$

where  $h$  is Planck's constant,  $T_{\text{meas}}$  is the measurement time, and  $N$  is the number of independent measurements [14].<sup>1</sup> Equation (3) is a specific case of a general property of atomic sensors in which the minimum detectable field is proportional to the minimum resolvable phase shift and inversely proportional to the product of the measurement time and the interaction strength [16]. This relationship is often referred to as the atom shot noise limit due to the probabilistic nature of the measurement's projection of the atomic wavefunction.

The definition in (3) must be adjusted when the measurement time is longer than the dephasing time  $T_2$ . To account for this,  $T_{\text{meas}}$  is taken to be  $T_2$ , and the number of independent measurements is taken to be  $N = N_a T_{\text{int}}/T_2$ , where  $T_{\text{int}}$  is the total integration time and  $N_a$  is the average number of excited Rydberg atoms, each of which participates in the measurement over time  $T_2$ . Therefore, the atom shot noise limit becomes

$$E_{\text{min}} = \frac{h}{|\bar{\mu}_{\text{RF}}| \sqrt{N_a T_{\text{int}} T_2}}. \quad (4)$$

When quoting values for the electric field sensitivity  $E_{\text{min}}$ , the units may be given in electric field strength, e.g., V/m, as calculated from (4), where the bandwidth of the measurement ( $1/T_{\text{int}}$ ) has been specified. Alternatively, sensitivity can also be specified in units of V/m/ $\sqrt{\text{Hz}}$ , where a bandwidth has not been assumed. It is important to recognize that the dependence  $E_{\text{min}} \propto 1/\sqrt{T_{\text{int}}}$  in (4) is only valid for the case where the measurement time is longer than  $T_2$ . This dependence of the field sensitivity on the square root of the measurement bandwidth is the same for traditional receivers. For higher bandwidth measurements (e.g., when using modulated signals for communications), the sensitivity scaling of atomic electric field sensors is substantially altered [i.e., see (3)], and it no longer behaves like white noise.

The density of Rydberg atoms within a given volume is limited by the blockade radius, and the total number of Rydberg atoms is limited by the overlap between the optical fields and that volume. The number of Rydberg atoms  $N_a$  has been estimated to be between 100 [10] and 1000 [17] atoms in recent experiments, which is much lower than the limit set by the blockade radius. Higher atom numbers could be obtained with access to higher laser powers and/or specialized magneto-optical traps (e.g., anisotropic).

For warm atoms, the decoherence rate is generally limited by transit time broadening, i.e., the time it takes for atoms to leave the cross-sectional area of the optical fields. The transit-time-induced decoherence rate is a function of the particular beam width and atomic temperature used in a given experiment; this rate is estimated to be around  $2\pi \times 370$  kHz ( $2\pi \times 37$  kHz) for a  $100 \mu\text{m}$  (1 mm)  $1/e^2$  intensity beam waist at room temperature [22]. For cold atoms, because the atoms can remain within the optical cross section for a much

longer duration, transit time broadening is no longer the dominant decoherence mechanism. In an ideal case, the natural and thermally induced decay processes can be the limiting factors in the decoherence time for a given measurement. Based on the calculated total lifetime  $\tau_{\text{total}}$ , the decoherence rate for cold atoms in this case (where  $T_2 \approx \tau_{\text{total}}$ ) can be between approximately 1 kHz and 1 MHz depending on  $n$ , as well as other possible sources of noise.

The Rydberg atom sensor can also measure incident RF/microwave fields that are off-resonant from a transition to |4). This is done by measuring the change of a spectroscopic feature associated with an atomic energy state due to the AC Stark shift [1]. The off-resonant AC Stark shift measurement technique is distinct from, and less sensitive than, the resonant Autler–Townes technique where the spectroscopic peak splits in two. Techniques used for detecting off-resonant fields include a heterodyne detection scheme [4], [9], [11] or a self-calibrating instrument that measures the bare AC Stark shift [2], [10]. These techniques have recently been investigated experimentally for precision metrology [2] and ultra-wideband spectrum analysis [11].

### III. ATOMIC ELECTRIC FIELD SENSORS COMPARED TO TRADITIONAL ELECTROMAGNETIC RECEIVERS

Traditional electromagnetic receivers consist of a receiving antenna and electronic front-end. Antennas absorb energy from an electromagnetic field and convert these free-space modes into guided modes, generating a current that can be amplified, filtered, and rectified in front-end electronics before being processed in the analog or digital domains by a user. Atomic electric field sensors do not mandate any net absorption of the incident electric fields; instead, via a coherent process, incident electric fields alter the internal states of Rydberg atoms, which are then imparted to an optical field as amplitude or phase modulations and detected spectroscopically. Due to these fundamental differences, some of the typical parameters used to describe traditional electromagnetic receivers (e.g., gain and power sensitivity) do not have a well-defined counterpart in atomic electric field sensors. However, both types of receivers can be characterized in terms of electric field sensitivity, selectivity, channel capacity, and dynamic range. This section compares performance characteristics of traditional receivers and atomic electric field sensors to provide a better understanding of the advantages and limitations of the atomic electric field sensor.

#### A. SOURCES OF NOISE

All electromagnetic sensors are affected by internal and external sources of noise. Internal sources can include fundamental quantum limits as well as practical sources of noise in electronic components. External sources can include blackbody radiation, interference, or other signals from nearby communications sources. This article focuses primarily on internal sources of noise in order to compare the sensitivity limits of traditional receivers to those of atomic electric field sensors.

<sup>1</sup>The Python package ARC-Alkali-Rydberg-calculator has built-in functions for calculating the dipole moment and lifetime for a given transition [15].



### 1) NOISE AFFECTING TRADITIONAL RECEIVERS

The internal noise floor of traditional receivers is generally limited by the noise produced from the various components in the front-end electronics. The noise power of the full system is described by the noise equivalent circuit, which accounts for any external noise picked up by the antenna (which is neglected here), as well as internal noise generated by the feed line, amplifier, filter, and any other active or passive components in the front-end.

The noise power is  $P_N = k_B T_{eq} B$ , where  $k_B$  is Boltzmann's constant,  $T_{eq}$  is the equivalent noise temperature of the system, and  $B$  is the bandwidth of the measurement. The equivalent noise temperature depends on the noise power added by each component in the receiver system as well as the gains and losses at each stage [18]. In practice, the equivalent noise temperature of the internal receiver components is generally dominated by transistor noise in the front-end amplifier, which includes thermal and shot noise contributions.

### 2) NOISE AFFECTING ATOMIC ELECTRIC FIELD SENSORS

The total noise of an atomic electric field sensor has a number of contributions: noise causing a variation in the number of atoms, noise on the optical fields, and noise in the signal recovery path (photodetector and electronics). For the atomic electric field sensor, the primary sources of noise are typically those associated with the atoms and the optical fields. Atomic electric field sensors can operate with sufficient power in the detected optical field such that the signal received by the photodetector is higher than electronic noise in the remainder of the signal recovery electronics, though it is important to recognize that this requires careful design to ensure that the power transmitted by the EIT process is sufficiently high. The limiting noise source for atomic electric field sensors is, therefore, not the minimum noise floor of the electronics (as is the case in traditional receivers); rather, it is the resolvability of the characteristic spectral features that arise due to the presence of an external electric field. This is fundamentally limited by the atom shot noise limit, but in practice is generally limited by other factors.

In current systems, the ability to resolve spectral features is often limited by photon shot noise of the optical readout [3], [11]. (However, because the number of detected photons per Rydberg atom can be made high, the sensor performance can theoretically reach the atom shot noise limit.) Other factors impacting the spectral resolution of the measurement may include the resolution bandwidth of the detector,  $1/f$  noise on the detector, and broadening effects in the atoms (such as Doppler or transit broadening). The most sensitive electric field measurements to date employ heterodyne techniques [1], [11], [19] where  $1/f$  noise is not dominant. Carefully chosen beam geometries can minimize Doppler broadening, and using a vapor cell with a buffer gas or special coating can minimize some collisional broadening effects, though Rydberg atoms will still be highly sensitive to any collisions. Employing laser-cooled atoms can also

minimize certain decoherence effects, e.g., those due to transit time broadening.

## B. ELECTRIC FIELD SENSITIVITY

The sensitivity of traditional receivers is often described with respect to received power. However, because Rydberg atoms are fundamentally electric field sensors, the electric field sensitivity metric is used here to allow for direct comparisons. Power sensitivity comparisons are discussed in Section III-C. Intensity sensitivity is another metric that may be used to describe both the performance of atomic electric field sensors [20], [21] and that of traditional receivers, especially in systems where the antenna cannot be characterized separately from the electronics.

### 1) SENSITIVITY OF TRADITIONAL RECEIVERS

The minimum signal electric field strength required to match the noise floor  $P_N$  of a traditional receiver is a function of the size, shape, and efficiency of the antenna. The present analysis assumes a lossless center-fed halfwave dipole antenna. Average power is related to the electric field amplitude via  $P/A_d = I = \epsilon_0 c |E|^2 / 2$ , where  $A_d$  is the effective area of the dipole antenna,  $I$  is the intensity,  $\epsilon_0$  is the permittivity of free space,  $c$  is the speed of light, and  $|E|$  is the electric field amplitude. The effective area  $A_d = G_d \lambda^2 / (4\pi)$ , where  $G_d = 1.64$  is the directivity of a lossless halfwave dipole antenna and  $\lambda$  is the wavelength of radiation. The electric field amplitude that must be applied to a lossless dipole antenna with effective area  $A_d$  in order to match the noise floor is then  $|E_N| = \sqrt{2P_N / (\epsilon_0 c A_d)}$ .

Fig. 5(a) shows the electric field sensitivity of a traditional receiver in a 1 Hz bandwidth assuming  $T_{eq} = 290$  K, for which  $P_N = -174$  dBm. The sensitivity of practical systems may be higher or lower than this particular example depending on the actual front-end components, the receiver topology, and the level of external noise coupling into the receiver.

The scaling of the electric field sensitivity with carrier frequency [ $E_{min} \propto \nu$  shown in Fig. 5(a)] is based on the assumption that the antenna aperture size is optimized to  $\lambda/2$  for each carrier frequency  $\nu = c/\lambda$ , i.e., the electric field strength required to overcome a fixed  $P_N$  is larger for smaller antennas. This is equivalent to stating that the minimum detectable power scales as  $P_{min} \propto 1/\lambda^2$ .

### 2) SENSITIVITY OF ATOMIC ELECTRIC FIELD SENSORS

The electric field sensitivity for the atomic sensor is calculated from (4) and shown in Fig. 5 for the example parameters defined in the caption. The calculation of the discrete carrier frequencies for the atomic electric field sensor is described in the Appendix.

As seen in Fig. 5(a), it is apparent that the atomic electric field sensor is less sensitive than a traditional halfwave dipole antenna receiver system at  $T_{eq} = 290$  K for most carrier frequencies. It is not expected that the electric field sensitivity of

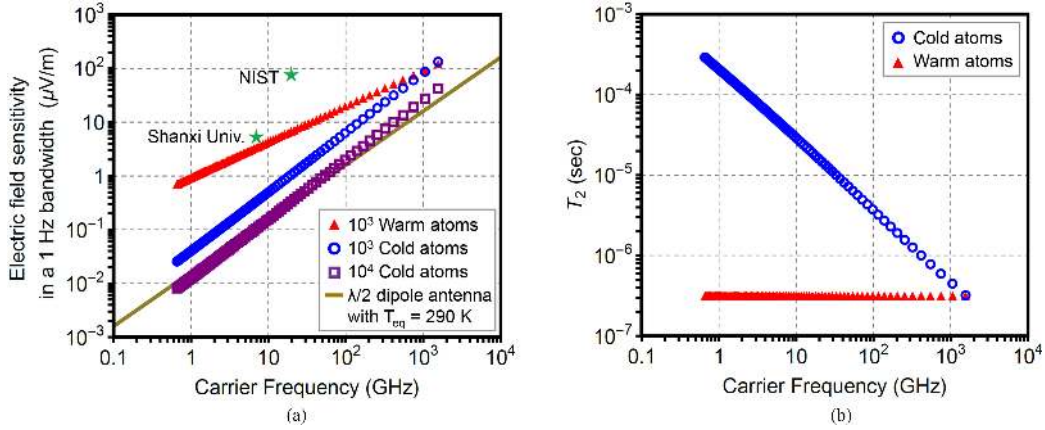


**FIGURE 5.** (a) Electric field sensitivity as a function of carrier frequency for two experimentally measured data points from [1] (NIST) and [19] (Shanxi University) and theoretical predictions for the cases defined in the legend. The atomic electric field sensor theoretical predictions are for the  $nD_{5/2} \rightarrow (n+1)P_{3/2}$  Rydberg transitions in cesium with  $10 \leq n \leq 100$ . The warm atom case assumes  $N_a = 1000$  atoms and a decoherence time of  $0.3 \mu\text{s}$  [4]. The two cold atom cases assume different atom numbers ( $N_a = 10^3$  and  $10^4$  atoms) and a decoherence time calculated from [15] and shown in (b). Because the cold atom decoherence time varies with  $n$ , these points have a different trend than the warm atom case. The solid gold curve shows the  $T_{\text{eq}} = 290$  K sensitivity of an ideal halfwave dipole antenna optimized for each carrier frequency. (b) Decoherence time  $T_2$  used in (a) for cold and warm atoms. In the warm atom case, a constant transit-time-limited lifetime is assumed. In the cold atom case, the lifetime is assumed to be limited only by natural and blackbody radiation-induced decay processes.

atomic electric field sensors using warm atom vapors will be able to match that of a lossless dipole antenna-based receiver at  $T_{\text{eq}} = 290$  K, but it may be comparable when accounting for the power losses and higher internal noise levels present in many practical systems. Power sensitivities may scale more favorably, which is discussed further in Section III-C. Further improvement of the sensitivity will require using higher atom numbers and/or reducing sources of decoherence. Cold atom systems could enable improved sensitivity compared to warm atom systems owing to the potential for longer coherence times. The effective sensitivity for both warm and cold atom-based sensors will still be limited in practical applications by any external sources of noise that fall within the sensor's bandwidth.

It is instructive to compare how the electric field sensitivity scales with carrier frequency,  $\nu$ , for these three types of sensors. The sensitivities exhibit different characteristic slopes as a function of  $\nu$  in Fig. 5(a).

In the warm atom case, the electric field sensitivity scales with the transition strength like  $E_{\text{min}} \propto 1/\mu_{\text{RF}}$  from (3). For large principal quantum number  $n$ , the transition frequency  $\nu$  between Rydberg states  $n$  and  $n+1$  scales as  $\nu \propto n^{-3}$ . The dipole moment  $\mu_{\text{RF}}$  scales with  $n$  as  $\mu_{\text{RF}} \propto n^2$ . Therefore, the electric field sensitivity scales with frequency as  $E_{\text{min}} \propto \nu^{2/3}$  in Fig. 5(a).

The cold atom case is more complex and has a different scaling with  $\nu$  because the decoherence rate  $T_2$  is no longer dominated by the transit time of the atoms through the optical fields, as is the case in warm atoms. The decoherence rate ( $1/T_2$ ) is fundamentally limited by the natural lifetime of the Rydberg state, but it is often faster in practice due to collisional broadening, transit-time broadening, or other sources of loss. To investigate the fundamental limits, the natural lifetimes of the Rydberg states can be calculated numerically [15] or estimated by  $\tau_{\text{nat}} \sim \tau_0 n^u$ , where  $n$  is the

**TABLE 1** Lifetime parameters for alkali atoms at zero temperature from [7]

Species	Parameter	S	P	D	F
Rb	$\tau_0$ (ns)	1.43	2.76	2.09	0.76
	$u$	2.94	3.02	2.85	2.95
Cs	$\tau_0$ (ns)	1.43	4.42	0.96	0.69
	$u$	2.96	2.94	2.93	2.94

principal quantum number and the values of  $\tau_0$  and  $u$  are shown in Table 1 for various atomic species and momentum states at zero temperature [7]. In practice,  $\tau_{\text{nat}}$  will be shorter at nonzero temperatures.

Blackbody radiation is a source of thermal noise that can impact the Rydberg atom decay rate. The blackbody radiation-induced decay rate  $1/\tau_{\text{bbr}}$  can be incorporated into the total decay rate by

$$\frac{1}{\tau_{\text{total}}} = \frac{1}{\tau_{\text{nat}}} + \frac{1}{\tau_{\text{bbr}}} \quad (5)$$

where  $\tau_{\text{bbr}}$  can be calculated based on transitions to neighboring states [15] or estimated by  $\tau_{\text{bbr}} = 3hn^2/(4\alpha^3 k_B T)$  [7]. Here,  $\alpha$  is the fine structure constant. The blackbody radiation-induced decay rate ( $1/\tau_{\text{bbr}}$ ) is linearly proportional to the absolute temperature  $T$  of the radiative environment, which here is taken to be room temperature. The total decay time in the idealized cold atom case where  $T_2 = \tau_{\text{total}}$  is shown in Fig. 5(b).

For cold atoms, the scaling of the electric field sensitivity with frequency can be estimated from the warm-atom relationship  $E_{\text{min}} \propto \nu^{2/3}$  described previously and noting that there is an additional dependence on  $\nu$  present in (4) due to the dependence of  $T_2$  on  $\nu$ . For the case where blackbody radiation dominates  $T_2$ , there is an additional scaling of  $E_{\text{min}} \propto \nu^{1/3}$ , and the sensitivity would scale linearly as  $E_{\text{min}} \propto \nu$  if this were the only additional factor. However,

the additional dependence of  $\tau_{\text{nat}}$  on  $n^u$  results in a more complex scaling with respect to  $\nu$ , which is evidenced by the slight deviation from linearity in the cold atom points shown in Fig. 5(a).

**C. POWER SENSITIVITY**

It is not straightforward to calculate a power sensitivity for the atomic electric field sensor. To convert from an electric field sensitivity to a power sensitivity, it is necessary to define the appropriate sensing area. This is a current topic of research [4], [11].

To better understand the importance of determining an accurate sensing area, it is instructive to assume an example sensing area for the atomic electric field sensor. One could assume a conservative sensing area equal to the cross section of the optical fields propagating through the atomic vapor. For a 1 mm × 1 cm interaction region and the measured sensitivity of 79  $\mu\text{V}/\text{m}/\sqrt{\text{Hz}}$  [1], the estimated power sensitivity is approximately -131 dBm in a 1 Hz bandwidth. However, with a smaller assumed sensing area, the atomic electric field sensor’s estimated power sensitivity is correspondingly smaller.

For an atom-shot-noise-limited electric field sensitivity of 100 nV/m/ $\sqrt{\text{Hz}}$  and an assumed sensing area of 1 mm × 1 cm, the projected power sensitivity is approximately -189 dBm in a 1 Hz bandwidth—well below the room temperature thermal noise limit of -174 dBm. Atomic electric field sensors, therefore, have the potential to surpass the room temperature thermal-noise-limited power sensitivity for the most sensitive detection regimes, especially for sensors employing heterodyne detection and methods to increase atom number and reduce decoherence (e.g., using optical cavities [22] and/or cold atoms).

**D. SELECTIVITY**

The selectivity of a receiver is often characterized in terms of the  $Q$ -factor, which is defined as  $Q = \nu/\Delta\nu$ , where  $\nu$  is the carrier frequency and  $\Delta\nu$  is the instantaneous bandwidth. The  $Q$ -factor of atomic electric field sensors is shown in Fig. 6 alongside some example electronic filters. The atoms provide a naturally narrowband response of approximately  $\Delta\nu = 10$  MHz [23], [24]. The  $Q$ -factor for traditional front-end electronic filters shown in Fig. 6 is defined only for the RF front-end stage (i.e., the antenna and any initial filter before the low-noise amplifier). In both standard RF front-ends and atomic electric field sensors, one can use analog and digital domain signal processing techniques in the intermediate frequency and/or digital stages, respectively, to achieve narrower instantaneous bandwidths.

To achieve high  $Q$ -factors, traditional receivers require specialized preselection filters, which have a limited linear tuning range and sensitivity degradation. These receivers typically operate with  $Q$ -factors around 10 (for halfwave dipoles) to 100 (for electrically small antennas), with specialized filters sometimes enabling  $Q$ -factors on the order of  $10^3$  [25]. In general, for frequencies above the super high

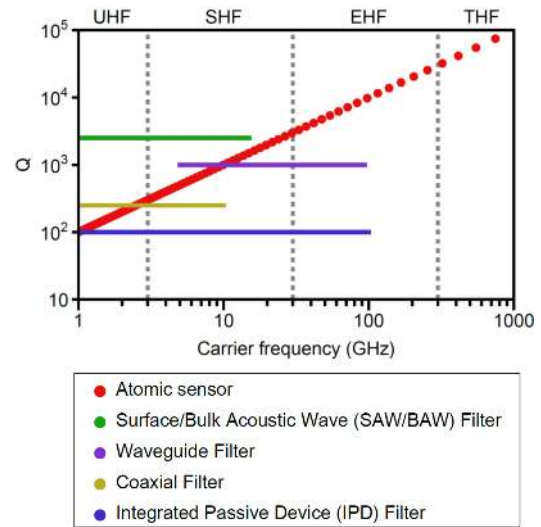


**FIGURE 6.**  $Q$ -factor of atomic electric field sensors and receiver front-end filters as a function of carrier frequency. The case of atomic electric field sensors, where the instantaneous bandwidth is approximately 10 MHz [23], [24], is shown in red points. The other lines show  $Q$ -factors for the standard front-end filters defined in the legend. See [25] for filter specifications.

frequency (SHF) band, it is difficult to achieve high- $Q$  filtering. Atomic electric field sensors have a comparable  $Q$  to standard front-end electronics for UHF and SHF frequencies. However, they maintain a naturally high- $Q$  response into the extremely high frequency band, as shown in Fig. 6. This narrowband response can enable resiliency against interference signals, which is discussed further in Section VI.

Similar to traditional receiver systems, additional analog and digital domain processing techniques can enable reduction of the effective instantaneous bandwidth. The  $Q$ -factor shown in Fig. 6 defines only the RF and analog filtering components of any receiver architecture. One can engineer a version of the atomic electric field sensor that is analogous to a heterodyne receiver architecture, which is discussed further in Section III-I. In the heterodyne case, the atomic electric field sensor has been shown to achieve a frequency resolution of less than 1 Hz [1], [19]. For the low-frequency bands, the atomic electric field sensor has a very small effective  $Q$  because the instantaneous bandwidth of the atoms is still approximately 10 MHz.

**E. POLARIZATION AND VECTOR ACCURACY**

The direction-of-arrival of a signal can be fully determined from measurement of the incident field’s amplitude and phase in three mutually orthogonal directions [26]. Atomic electric field sensors have been measured to have an amplitude precision of less than 1% [2], a phase accuracy of less than 0.1% [27], and a polarization accuracy of less than 0.5° [28]. Atomic electric field sensors have not yet been engineered to simultaneously sense three mutually orthogonal axes, though one recent work showed that by rotating a single-axis probe, one can infer vector information from a constant, stationary emitter [2]. In addition, another recent



**TABLE 2** Measurements of channel capacity for atomic electric field sensors

Frequency band(s)	Measured channel capacity
HF – VHF	40 Mbits/s for 30 MHz carrier [10]
SHF	8.2 Mbits/s for 17 GHz carrier [30]

demonstration measured the angle-of-arrival of an incoming signal by constructing a two-component atomic sensor array [6].

Comparable polarization accuracies are achievable with traditional receiver systems, though full vector antennas can become fairly large for frequencies below UHF with volumes on the order of the cube of the carrier wavelength. Additional research is needed to determine the accuracy limitations of the atomic electric field sensor for vector measurements in the off-resonant sensing regimes.

### F. CHANNEL CAPACITY

The atomic electric field sensor is limited in its channel capacity for higher frequency bands, especially in the regime where it is the most sensitive (UHF to THF). Examples of the measured channel capacity of the atomic electric field sensor for different frequencies are shown in Table 2. For low signal-to-noise ratios (SNRs), the channel capacity is roughly limited by the instantaneous bandwidth of the light-atom interaction according to the Shannon–Hartley theorem. Atomic electric field sensors have an instantaneous bandwidth of approximately 10 MHz, though one recent demonstration showed that this could potentially be expanded to 200 MHz for higher electric field strengths [29].

The atomic electric field sensor is capable of performing quadrature measurements of an incident RF field and, thus, can be used for receiving quadrature-encoded information. An initial demonstration of an 8-state phase-shift-keying protocol with the atomic electric field sensor measured an empirical channel capacity of 8.2 Mbits/s for a carrier frequency of 17 GHz [30].

For lower frequency bands, the atomic electric field sensor operates in the off-resonant regime with reduced sensitivity. However, the sensor is capable of operating with fairly high channel capacities in this regime; an empirical maximum channel capacity of 40 Mbits/s for a carrier frequency of 30 MHz was recently measured using the atomic electric field sensor [10].

The narrowband response of the atoms provides opportunities for lower bandwidth communications in crowded or contested electromagnetic environments with rates sufficient for audio and positioning data.

### G. DYNAMIC RANGE

The atomic electric field sensor can have limited dynamic range for the resonant mode of operation (for discrete frequencies between UHF and THF). However, it can achieve a very large dynamic range with a heterodyne technique or for the less-sensitive off-resonant mode of operation. Table 3 lists the dynamic range for different operating regimes of the

**TABLE 3** Estimated dynamic range for three operating regimes of the atomic electric field sensor from [1], [2], [11], [19], [31]

Detection technique	Autler-Townes (direct detection)	Heterodyne	AC Stark / Floquet
Electric field strengths	$\lesssim 10^{-3}$ V/m [31] to $< 1$ V/m	$\lesssim 10^{-5}$ V/m to $< 1$ V/m [1]	$\sim 1$ V/m to 10 kV/m [2]
Dynamic range (power)	10 dB	80 dB	80 dB
Atomic response	Resonant (narrowband)	Heterodyne	Off-resonant

atomic electric field sensor from [1], [2], [11], [19], [31]. The Rydberg atom electric field probe from Rydberg Technologies, Inc. can access the Autler–Townes through Floquet regimes and achieves a dynamic range of more than 80 dB for the latter [2]. Additional research and development is required to make smooth transitions among these operating regimes, especially for modulated signals.

### H. GAIN

The definition of gain for an atomic electric field sensor is fundamentally different than that for a traditional receiver. In a traditional receiver, there are two categories of contributions to the overall gain: the directivity of the antenna and amplification in the electronics. The directivity of the atomic electric field sensor is similar to that of an infinitesimal dipole (for which  $G = 1.5$ ) in that there is a well-defined polarization of the atomic electric dipole. In addition, similar to traditional receivers, the sensitivity of an atomic electric field sensor can be enhanced if one uses an antenna to focus an incident field and generate a higher intensity in the detection region [11].

In regards to amplification, while the atomic electric field sensor will generally have electronic gain elements (e.g., in the photodiode), it also has a separate means for amplification that does not scale in the same way as electronic components. Specifically, the gain of atomic electric field sensors can be enhanced by increasing the atom number, which gives rise to enhanced sensitivity owing to the distinct scaling of atom number with signal and noise.

### I. EXAMPLES OF RECEIVER ARCHITECTURES

The atomic electric field sensor can be constructed with receiver architectures that are in many ways analogous to specialized front-end electronics for traditional receiver systems. Two example architectures are shown in Fig. 7: an amplitude-modulation (AM) architecture and a heterodyne architecture. The best experimentally measured electric field sensitivity for the atomic AM receiver architecture is approximately  $300 \mu\text{V/m}/\sqrt{\text{Hz}}$  [3]. The RF heterodyne architecture shown in Fig. 7 is more complicated, but it enables better sensitivity with recently reported measurements of  $5.5 \mu\text{V/m}/\sqrt{\text{Hz}}$  [19] and  $79 \mu\text{V/m}/\sqrt{\text{Hz}}$  [1]. This RF heterodyne detection scheme uses a local oscillator resonant with



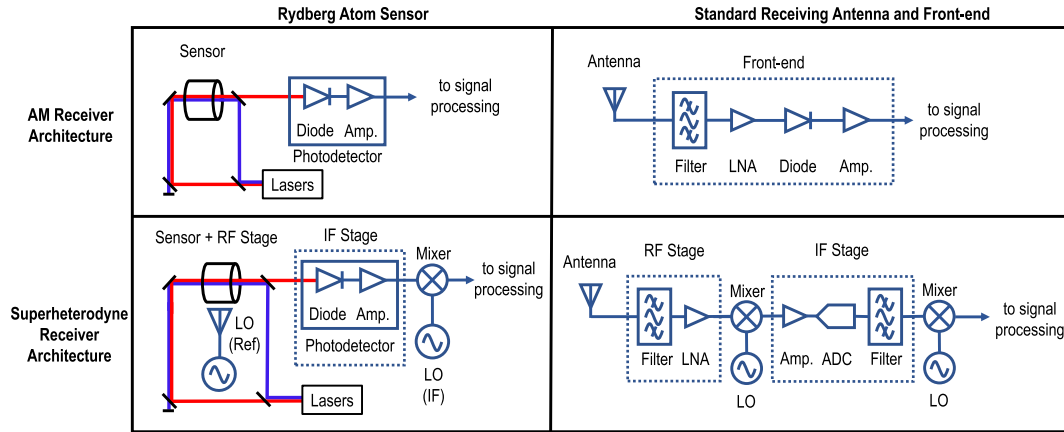


**FIGURE 7.** Two example receiving architectures for the atomic electric field sensor and a standard antenna and front-end. The top row shows the schemes for simple AM signal detection, and the bottom shows a version of heterodyne detection. (Note: The use of two local oscillators at different frequencies is sometimes referred to as superheterodyne detection.) The block diagrams on the right-hand side are adapted from [33].

the transition  $|3\rangle \leftrightarrow |4\rangle$ , and the incoming signal field has a small detuning relative to the local oscillator frequency [1], [19].

**IV. ADVANTAGES OF THE ATOMIC ELECTRIC FIELD SENSOR**

**A. RESISTANCE TO INTERFERENCE**

There are three key atomic electric field sensor characteristics that enable resistance to strong interference signals: a high- $Q$  response (narrow instantaneous bandwidth), agile tunability to enable fast frequency hopping, and a physically small sensing element for improved shielding. High  $Q$ -factors can enable more robust performance in a noisy environment because the sensor will have a strong rejection of interference outside a narrow band. The  $Q$ -factor of atomic electric field sensors is shown in Fig. 6, where the atoms provide a naturally narrowband response that is independent of the carrier frequency. Despite this high  $Q$ -factor, it is also important to recognize that each Rydberg state is sensitive to multiple transitions, and thus out-of-band frequencies can still perturb a given measurement.

**B. SELF-INTERFERENCE MITIGATION**

Capabilities for resistance to background interference can also be applied to self-interference mitigation. Cosite and colocated self-interference refers to the deleterious effects of cross-coupling between spectrum-dependent systems that are in close proximity. An atomic electric field sensor could be operated in such a way so that it does not couple to colocated or nearby spectral emissions due to its narrow instantaneous bandwidth.

For communications at frequency bands above UHF, the limited  $Q$ -factor at high frequencies combined with reradiation of the antennas can give rise to cosite interference. The atomic electric field sensor has an intrinsically high  $Q$ -factor at high frequencies and is nonradiating, and it, thus, could be deployed as a primary or backup wireless receiver for

assured spectrum sensing for applications ranging from communications to radio navigation.

**C. BROAD TUNABILITY**

The atomic electric field sensor is also capable of broad tunability. Tuning the resonance of the atomic electric field sensor is achieved by small adjustments to the optical frequency of one of the lasers used to excite the atoms. The tuning time is a function of the magnitude of the desired frequency hop. For example, if one wishes only to tune to a nearby Rydberg state, this could potentially be accomplished via a fast (submicrosecond) step current adjustment to the laser head. If one wishes to tune much further (e.g., from near 1 GHz to near 100 GHz), it is likely that the temperature or phase-matching of the laser will need to be adjusted, and the tuning time could take multiple seconds or longer. Alternatively, one could use a separate laser system for fast tuning between two frequencies, but this would increase the size, power consumption, and cost of the sensor.

By comparison, tuning of traditional receivers can generally be done quickly, though the magnitude of the tuning range is more limited than that for atomic electric field sensors. For example, the Keysight N5194A Agile Vector Adapter is a fast-hopping traditional solution, which can perform frequency hopping from 10 MHz to 40 GHz in less than ten microseconds [32]. However, traditional receivers achieve fast tuning by adjusting the local oscillator frequency and generally do not deliver fast tuning of the antenna or preselection filters themselves, which can leave them vulnerable to interferers across a wide spectral band. In addition, traditional receiver front-end components (viz. antenna, filter, low-noise amplifier, and mixer) have limited tuning ranges due to impedance matching requirements to maintain sensitivity performance and to avoid undesired circuit implementation parasitics and/or undesired signal propagation modes. The atomic electric field sensor uniquely offers broad tunability across multiple spectral bands.

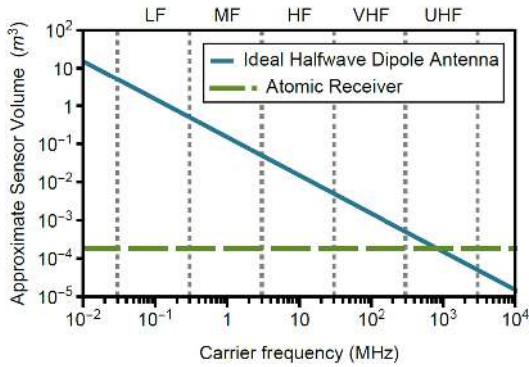


**FIGURE 8.** Approximate volume of halfwave dipole antennas (assuming volume =  $[G_d \lambda^2 / (4\pi)] \times 10$  cm, where  $G_d = 1.64$  is the gain of a lossless halfwave dipole antenna) and the volume of the atomic electric field sensor head (receiving element only, excluding lasers and electronics) developed by Rydberg Technologies, Inc. [2].

#### D. SENSOR SIZE

The atomic electric field sensor head is significantly smaller than typical antennas for carrier frequencies below approximately 1 GHz, as shown in Fig. 8. The atomic electric field sensor employs a small, compact sensor head that is broadly tunable, whereas the aperture size of traditional antennas generally scales with the wavelength of the radiation.

With further advances in laser miniaturization and photonic integration, the full sensor (including requisite lasers and electronics) could be contained in a volume of approximately 20 L in the near-term ( $\sim 10$  years) and potentially be made as small as a hand-held-size device in the long-term by employing excitation techniques requiring only diode lasers [8]. This size reduction would enable interference resistance capabilities for frequencies below 1 GHz not obtainable on many size-constrained platforms.

#### E. PROTECTION FROM INTENSE FIELD EVENTS

Atomic electric field sensors may also be engineered for resilience against intense field events such as electromagnetic pulses. The sensor head itself can be constructed without electronically conductive channels. In particular, it contains only glass optics and fiber optics as well as a glass or crystal vapor cell. The sensor head can be connected via optical fiber to a shielded box that houses the lasers and other requisite electronics. Hence, due to the absence of exposed electrical antenna and transmission lines, which are connected to voltage-biased electrical components with voltage handling limits, the atomic sensor could continue to function normally after an intense field event.

#### V. LIMITATIONS OF THE ATOMIC ELECTRIC FIELD SENSOR

The principal current limitation of an atomic electric field sensor compared to a traditional receiver is its relative lack of maturity. At present, these are highly specialized devices, with only one small company commercializing custom units [2]. Traditional RF/microwave receivers, on the

other hand, are commodity items, integrated in several instantiations in every mobile phone and many other devices on the planet. There are several technical hurdles that must be overcome to make atomic sensors more affordable and deployable. The primary technological hurdle at present is the lack of maturity of the visible control laser (at 480 nm for Rb and 510 nm for Cs). Improvements in narrow-linewidth, high-efficiency lasers at these wavelengths will be required for future Rydberg atom electric field sensor deployment.

The key limitations of atomic electric field sensors are summarized in Table 4. The atomic electric field sensor cannot replace traditional receivers for the majority of applications; rather, it should be viewed as an emerging technology with unique capabilities that can be exploited to improve or enable certain capabilities. Because the tuning time is limited by the time it takes to adjust the laser frequency, the sensor will operate most efficiently in situations where the carrier frequency is known.

Standard tactical communications often require channel capacities greater than 10 MHz, which cannot be achieved with a single atomic electric field sensor. (Multiple channels could be used with carrier aggregation to achieve larger channel capacities, but this comes at the expense of greater size, power, and cost.) In addition, traditional front-end filters can provide low-frequency selectivity with high  $Q$ -factors typically ranging from approximately 100 to 2500. Atomic electric field sensors have a fixed instantaneous bandwidth of approximately 10 MHz and, thus, cannot achieve the same preselection filtering for low carrier frequencies (e.g., below 1 GHz). However, similar to traditional receivers, the instantaneous bandwidth of atomic electric field sensors can be adjusted in digital signal processing provided that the interference signal does not distort or degrade sensor performance prior to analog-to-digital signal conversion. Additional examples of applications for which it would be challenging or impossible to use the atomic electric field sensor are discussed further in Section VI.

#### VI. APPLICATIONS

The atomic electric field sensor cannot offer continuous tunability for sensitivity levels required for many communications and sensing applications. However, it does offer some unique advantages for cosite mitigation, as described in Section IV-B, as well as in electromagnetic spectrum situational awareness, distributed sensing, and precision characterization of custom antennas.

##### A. ELECTROMAGNETIC SPECTRUM SITUATIONAL AWARENESS

The atomic electric field sensor's precision vector capabilities can identify the direction-of-arrival of an unknown RF/microwave field. In addition, while typical ultra-wideband antennas require careful optimization and impedance matching to minimize power losses and maintain sensitivity, the optical detection of the atomic electric field

**TABLE 4** Limitations of atomic electric field sensors

Characteristic	Traditional Antennas + Front-ends	Atomic Electric Field Sensors
Maturity	Commodity items	Ongoing basic research and emerging early prototypes
Cost	From pennies to $\approx$ \$200k, depending on front-end filtering requirements and complexity	Likely \$200k-\$500k (estimated) for early prototypes
Size	Very small for high frequencies	Near-term (long-term): Will be larger than standard antennas for frequencies UHF (SHF) and above. Significant laser miniaturization and photonic integration efforts are required.
Power consumption	Depends on front-end requirements (e.g., local oscillator needs)	Current laser systems require $\gtrsim$ 100 W of electrical power
Tunability	Can have thermal-noise-limited sensitivity for continuous frequencies within a given band of interest	Optimal sensitivity only achievable among discrete frequencies from $\approx$ 1 – 500 GHz. (Continuous tunability down to near-DC has worse sensitivity.)
Channel capacity	Limited by instantaneous bandwidth and signal-to-noise ratio (SNR)	Instantaneous bandwidth is limited to approximately 10 MHz
Deployment	Central technology for all communications	Not yet deployable outside benign laboratory environments

sensor is naturally impedance-matched for all available sensing frequencies.

For situations where the field strength is sufficiently strong, the atomic electric field sensor is theoretically continuously tunable from near-DC through THz carrier frequencies. One recent demonstration showed that the atomic electric field sensor can measure fields as low as  $300 \mu\text{V/m}$  in the ultra low frequency (ULF) band (from 600 Hz–1.5 kHz in this experiment) [9]. Another recent theoretical analysis showed that the atomic electric field sensor can measure field strengths of  $\lesssim 10^2 \text{ V/m}$  for carrier frequencies from 1 kHz through approximately 50 MHz, which spans the ULF through very high frequency (VHF) bands [4]. There was also a separate recent experimental demonstration showing proof-of-principle continuous tunability from the very low frequency through high-frequency (HF) bands [10].

The sensitivity of the atomic electric field sensor can theoretically be made comparable to electrically small antennas in the ULF through VHF bands [4], and thus, it could similarly be used for communications and sensing applications requiring small-size sensing elements, but with the added advantage of having nonreradiating receivers.

### B. DISTRIBUTED SENSING

Atomic electric field sensors can enable higher precision distributed sensing, e.g., for radar and geolocation, with a lower SWaP sensor head. Owing to the deeply subwavelength sensing capability of atomic electric field sensors, they can improve the phase and spatial resolution for distributed sensing applications such as bistatic radar. In addition, a version of the atomic electric field sensor could be engineered to sense two or more vastly disparate frequencies (e.g., 10 MHz and 10 GHz), which can enable spectrally sparse multitone measurements—a common technique to overcome weather-induced decoherence.

### C. PRECISION CHARACTERIZATION OF CUSTOM ANTENNAS

Custom antennas can enable the generation of novel geometries and can also reduce the size and weight of traditional

receivers. However, characterizing the field of these custom antennas and identifying defects can be difficult due to the mutual interference between the custom antenna and the characterization antenna. The atomic electric field sensor is composed of dielectric material that does not generate mutual interference effects. For research and standards development, the atomic electric field sensor has an SI-traceable measurement capability (i.e., one that is characterized by a fundamental constant), and it can enable absolute electric field measurement uncertainties of less than 1%, which is nearly an order of magnitude better than current antenna standards [2], [34]. The partially miniaturized atomic electric field probe from Rydberg Technologies, Inc. is continuously tunable from 10 MHz (HF) to just under 1 THz (THF) [2] for high field strengths, which is sufficient for precision antenna characterization applications.

## VII. CONCLUSION AND OUTLOOK

This review has presented a comprehensive perspective on the capabilities and outlook of Rydberg atom electric field sensors. Their advantages and limitations have been identified as a function of carrier frequency, and comparisons to traditional receiver characteristics have been made. With substantial laser advances, future miniaturization efforts, and application-specific research and development, atomic electric field sensors are projected to make an impact in spectrum situational awareness, communications, and sensing applications.

### APPENDIX

The Rydberg energy levels (relative to the ionization energy) are given by the Rydberg formula

$$E(n, j, l) = -\frac{hcRy}{(n - \delta(n, j, l))^2} \quad (6)$$

where  $Ry$  is the Rydberg constant [35]. The term  $\delta(n, j, l)$  is known as a quantum defect that gives rise to a new effective principal quantum number  $n_{\text{eff}} = n - \delta(n, j, l)$ , where  $n$  is the principal quantum number of the Rydberg state,  $j$  describes the total angular momentum, and  $l$  describes

**TABLE 5** Defects in cesium measured in [36] and [37]

State	Defect	Value	Ref.
$nS_{1/2}$	$\delta_0$	4.04935665(38)	[36]
	$\delta_2$	0.2377037	
$nP_{3/2}$	$\delta_0$	3.5589599	[37]
	$\delta_2$	0.392469	
$nD_{5/2}$	$\delta_0$	2.46631524(63)	[36]
	$\delta_2$	0.013577	
$nF_{7/2}$	$\delta_0$	0.03341424(96)	[36]
	$\delta_2$	-0.198674	

**TABLE 6** Defects in rubidium measured in [38] and [39]

State	Defect	Value	Ref.
$nS_{1/2}$	$\delta_0$	3.1311804(10)	[38]
	$\delta_2$	0.1784(6)	
$nP_{3/2}$	$\delta_0$	2.6416737(10)	[38]
	$\delta_2$	0.2950(7)	
$nD_{5/2}$	$\delta_0$	1.34646572(30)	[38]
	$\delta_2$	-0.59600(18)	
$nF_{7/2}$	$\delta_0$	0.0165437(7)	[39]
	$\delta_2$	-0.086(7)	

the orbital angular momentum. The quantum defects are approximated by  $\delta(n, j, l) \approx \delta_0 + \delta_2/(n - \delta_0)^2$ , where  $\delta_0$  and  $\delta_2$  are given in Tables 5 and 6 for cesium and rubidium, respectively. The Rydberg constant for cesium is  $Ry = 109\,736.862\text{ cm}^{-1}$ . The Rydberg constant for rubidium is  $Ry = 109\,736.605\text{ cm}^{-1}$ . In practice, not all Rydberg levels are accessible because transitions to high- $n$  Rydberg states have larger dipole moments and, thus, require higher optical powers to access. The present analysis only considers  $n \leq 100$  for this reason.

Equation (6) is a good approximation, though not exact, of the energy separation between Rydberg levels. It typically has an error of no more than 1 MHz, which is inside the bandwidth of interest. This formula is used to calculate the frequency separation between neighboring Rydberg levels, which enables sensing at RF/microwave frequencies.

## ACKNOWLEDGMENT

The authors would like to thank C. Davis, G. Jacyna, C. Niessen, and I. McMichael for helpful discussions. This work was supported by the MITRE Innovation Program. Approved for Public Release; Distribution Unlimited. Public Release Case Number 20-3470. ©2021 The MITRE Corporation.

## REFERENCES

[1] J. A. Gordon, M. T. Simons, A. H. Haddab, and C. L. Holloway, "Weak electric field detection with sub-1 Hz resolution at radio frequencies using a Rydberg atom-based mixer," *AIP Adv.*, vol. 9, no. 4, 2019, Art. no. 045030, doi: [10.1063/1.5095633](https://doi.org/10.1063/1.5095633).  
 [2] D. Anderson, R. Sapiro, and G. Raithel, "A self-calibrating SI-traceable broadband Rydberg atom-based radio-frequency electric field probe and measurement instrument," *IEEE Trans. Antennas Propag.*, to be published, doi: [10.1109/TAP.2021.3060540](https://doi.org/10.1109/TAP.2021.3060540).

[3] S. Kumar, H. Fan, H. Kübler, J. Sheng, and J. P. Shaffer, "Atom-based sensing of weak radio frequency electric fields using homodyne readout," *Sci. Rep.*, vol. 7, Feb. 2017, Art. no. 42981, doi: [10.1038/srep42981](https://doi.org/10.1038/srep42981).  
 [4] D. H. Meyer, Z. A. Castillo, K. C. Cox, and P. D. Kunz, "Assessment of Rydberg atoms for wideband electric field sensing," *J. Phys. B.*, vol. 53, no. 3, Jan. 2020, Art. no. 034001, doi: [10.1088/1361-6455/ab6051](https://doi.org/10.1088/1361-6455/ab6051).  
 [5] M. T. Simons, J. A. Gordon, and C. L. Holloway, "Fiber-coupled vapor cell for a portable Rydberg atom-based radio frequency electric field sensor," *Appl. Opt.*, vol. 57, no. 22, pp. 6456–6460, Aug. 2018, doi: [10.1364/AO.57.006456](https://doi.org/10.1364/AO.57.006456).  
 [6] A. K. Robinson, N. Prajapati, D. Senic, M. T. Simons, and C. L. Holloway, "Determining the angle-of-arrival of a radio-frequency source with a Rydberg atom-based sensor," 2021, *arXiv:2101.12071*.  
 [7] T. F. Gallagher, "Rydberg atoms," *Cambridge Monographs on Atomic, Molecular and Chemical Physics*. Cambridge, U.K.: Cambridge Univ. Press, 2005, doi: [10.1017/CBO9780511524530](https://doi.org/10.1017/CBO9780511524530).  
 [8] D. P. Fahey and M. W. Noel, "Excitation of Rydberg states in rubidium with near infrared diode lasers," *Opt. Exp.*, vol. 19, no. 18, pp. 17002–17012, 2011, doi: [10.1364/OE.19.017002](https://doi.org/10.1364/OE.19.017002).  
 [9] Y.-Y. Jau and C. Tony, "Vapor-cell-based atomic electrometry for detection frequencies below kHz," *Phys. Rev. Appl.*, vol. 13, May 2020, Art. no. 054034, doi: [10.1103/PhysRevApplied.13.054034](https://doi.org/10.1103/PhysRevApplied.13.054034).  
 [10] K. C. Cox, D. H. Meyer, F. K. Fatemi, and P. D. Kunz, "Quantum-limited atomic receiver in the electrically small regime," *Phys. Rev. Lett.*, vol. 121, Sep. 2018, Art. no. 110502, doi: [10.1103/PhysRevLett.121.110502](https://doi.org/10.1103/PhysRevLett.121.110502).  
 [11] D. H. Meyer, P. D. Kunz, and K. C. Cox, "Waveguide-coupled Rydberg spectrum analyzer from 0 to 20 GHz," *Phys. Rev. Appl.*, vol. 15, Jan. 2021, Art. no. 014053, doi: [10.1103/PhysRevApplied.15.014053](https://doi.org/10.1103/PhysRevApplied.15.014053).  
 [12] J. A. Gordon et al., "Millimeter wave detection via Autler-Townes splitting in rubidium Rydberg atoms," *Appl. Phys. Lett.*, vol. 105, no. 2, 2014, Art. no. 024104, doi: [10.1063/1.4890094](https://doi.org/10.1063/1.4890094).  
 [13] C. Holloway et al., "A multiple-band Rydberg atom-based receiver: AM/FM stereo reception," *IEEE Antennas Propag. Mag.*, to be published, doi: [10.1109/MAP.2020.2976914](https://doi.org/10.1109/MAP.2020.2976914).  
 [14] H. Fan, S. Kumar, J. Sedlacek, H. Kübler, S. Karimkashi, and J. P. Shaffer, "Atom based RF electric field sensing," *J. Phys. B.*, vol. 48, no. 20, Sep. 2015, Art. no. 202001, doi: [10.1088/0953-4075/48/20/202001](https://doi.org/10.1088/0953-4075/48/20/202001).  
 [15] N. Šibalić, J. D. Pritchard, C. S. Adams, and K. J. Weatherill, "ARC: An open-source library for calculating properties of alkali Rydberg atoms," *Comput. Phys. Commun.*, vol. 220, pp. 319–331, 2017, doi: [10.1016/j.cpc.2017.06.015](https://doi.org/10.1016/j.cpc.2017.06.015).  
 [16] J. Kitching, S. Knappe, and E. A. Donley, "Atomic sensors—A review," *IEEE Sensors*, vol. 11, no. 9, pp. 1749–1758, Sep. 2011, doi: [10.1109/JSEN.2011.2157679](https://doi.org/10.1109/JSEN.2011.2157679).  
 [17] E. G. Brekke, "Stimulated emission studies of ultracold Rydberg atoms," Ph.D. dissertation, Dept. Phys., Univ. Wisconsin-Madison, Madison, WI, USA, 2009.  
 [18] S. J. Orfanidis, *Electromagnetic Waves and Antennas*. Piscataway, NJ, USA: Rutgers Univ., 2016. [Online]. Available: <http://eceweb1.rutgers.edu/~orfanidi/ewa/>  
 [19] M. Jing et al., "Atomic superheterodyne receiver based on microwave-dressed Rydberg spectroscopy," *Nature Phys.*, vol. 16, pp. 911–915, Jun. 2020, doi: [10.1038/s41567-020-0918-5](https://doi.org/10.1038/s41567-020-0918-5).  
 [20] E. Paradis, G. Raithel, and D. A. Anderson, "Atomic measurements of high-intensity VHF-band radio-frequency fields with a Rydberg vapor-cell detector," *Phys. Rev. A.*, vol. 100, Jul. 2019, Art. no. 013420, doi: [10.1103/PhysRevA.100.013420](https://doi.org/10.1103/PhysRevA.100.013420).  
 [21] D. A. Anderson, E. G. Paradis, and G. Raithel, "A vapor-cell atomic sensor for radio-frequency field detection using a polarization-selective field enhancement resonator," *Appl. Phys. Lett.*, vol. 113, Aug. 2018, Art. no. 073501, doi: [10.1063/1.5038550](https://doi.org/10.1063/1.5038550).  
 [22] D. H. Meyer, "Magnetic and electric field sensing and applications based on coherent effects in neutral atoms," Ph.D. dissertation, Dep. Phys., Univ. Maryland, College Park, MD, USA, 2018.  
 [23] A. B. Deb and N. Kjærgaard, "Radio-over-fiber using an optical antenna based on Rydberg states of atoms," *Appl. Phys. Lett.*, vol. 112, no. 21, 2018, Art. no. 211106, doi: [10.1063/1.5031033](https://doi.org/10.1063/1.5031033).  
 [24] M. T. Simons, A. H. Haddab, J. A. Gordon, D. Novotny, and C. L. Holloway, "Embedding a Rydberg atom-based sensor into an antenna for phase and amplitude detection of radio-frequency fields and modulated signals," *IEEE Access*, vol. 7, pp. 164975–164985, 2019, Accessed: Jul. 21, 2020, doi: [10.1109/ACCESS.2019.2949017](https://doi.org/10.1109/ACCESS.2019.2949017).



- [25] K&L Microwave Catalog. Accessed: Jul. 21, 2020. [Online]. Available: <http://www.klmicrowave.com/>
- [26] E. L. Afraimovich, V. V. Chernukhov, V. A. Kobzar, and K. S. Palamartchouk, "Determining polarization parameters and angles of arrival of HF radio signals using three mutually orthogonal antennas," *Radio Sci.*, vol. 34, no. 5, pp. 1217–1225, Sep. 1999, doi: [10.1029/1999RS900042](https://doi.org/10.1029/1999RS900042).
- [27] M. T. Simons, A. H. Haddab, J. A. Gordon, and C. L. Holloway, "A Rydberg atom-based mixer: Measuring the phase of a radio frequency wave," *Appl. Phys. Lett.*, vol. 114, no. 11, 2019, Art. no. 114101, doi: [10.1063/1.5088821](https://doi.org/10.1063/1.5088821).
- [28] J. A. Sedlacek, A. Schwettmann, H. Kübler, and J. P. Shaffer, "Atom-based vector microwave electrometry using rubidium Rydberg atoms in a vapor cell," *Phys. Rev. Lett.*, vol. 111, Aug. 2013, Art. no. 063001, doi: [10.1103/PhysRevLett.111.063001](https://doi.org/10.1103/PhysRevLett.111.063001).
- [29] Z. Song *et al.*, "Rydberg-atom-based digital communication using a continuously tunable radio-frequency carrier," *Opt. Exp.*, vol. 27, no. 6, pp. 8848–8857, Mar. 2019, doi: [10.1364/OE.27.008848](https://doi.org/10.1364/OE.27.008848).
- [30] D. H. Meyer, K. C. Cox, F. K. Fatemi, and P. D. Kunz, "Digital communication with Rydberg atoms and amplitude-modulated microwave fields," *Appl. Phys. Lett.*, vol. 112, no. 21, 2018, Art. no. 211108, doi: [10.1063/1.5028357](https://doi.org/10.1063/1.5028357).
- [31] J. A. Sedlacek, A. Schwettmann, H. Kübler, R. Löw, T. Pfau, and J. P. Shaffer, "Microwave electrometry with Rydberg atoms in a vapour cell using bright atomic resonances," *Nature Phys.*, vol. 8, no. 11, pp. 819–824, Nov. 2012, doi: [10.1038/nphys2423](https://doi.org/10.1038/nphys2423).
- [32] Keysight Technologies, N5194 A and N5192 A UXG Agile Vector Adapter. Accessed: Jan. 7, 2020. [Online]. Available: <https://www.keysight.com/en/pcx-x2015003/signal-generators-signal-sources>
- [33] C. Bowick, J. Blyler, and C. Ajluni, Eds., *RF Circuit Design*, 2nd ed. Burlington, MA, USA: Newnes, 2008, pp. 185–201, doi: [10.1016/B978-075068518-4.50010-2](https://doi.org/10.1016/B978-075068518-4.50010-2).
- [34] C. L. Holloway *et al.*, "Broadband Rydberg atom-based electric-field probe for SI-Traceable, self-calibrated measurements," *IEEE Trans. Antennas Propag.*, vol. 62, no. 12, pp. 6169–6182, Dec. 2014, doi: [10.1109/TAP.2014.2360208](https://doi.org/10.1109/TAP.2014.2360208).
- [35] M. Mack *et al.*, "Measurement of absolute transition frequencies of  $^{87}\text{Rb}$  to  $nS$  and  $nD$  Rydberg states by means of electromagnetically induced transparency," *Phys. Rev. A*, vol. 83, May 2011, Art. no. 052515, doi: [10.1103/PhysRevA.83.052515](https://doi.org/10.1103/PhysRevA.83.052515).
- [36] K.-H. Weber and C. J. Sansonetti, "Accurate energies of  $nS$ ,  $nP$ ,  $nD$ ,  $nF$ , and  $nG$  levels of neutral cesium," *Phys. Rev. A*, vol. 35, pp. 4650–4660, Jun. 1987, doi: [10.1103/PhysRevA.35.4650](https://doi.org/10.1103/PhysRevA.35.4650).
- [37] C. J. Lorenzen and K. Niemax, "Precise quantum defects of  $nS$ ,  $nP$  and  $nD$  levels in  $\text{Cs I}$ ," *Zeitschrift Physik A*, vol. 315, no. 2, pp. 127–133, Jun. 1984, doi: [10.1007/BF01419370](https://doi.org/10.1007/BF01419370).
- [38] W. Li, I. Mourachko, M. W. Noel, and T. F. Gallagher, "Millimeter-wave spectroscopy of cold Rb Rydberg atoms in a magneto-optical trap: Quantum defects of the  $ns$ ,  $np$ , and  $nd$  series," *Phys. Rev. A*, vol. 67, May 2003, Art. no. 052502, doi: [10.1103/PhysRevA.67.052502](https://doi.org/10.1103/PhysRevA.67.052502).
- [39] J. Han, Y. Jamil, D. V. L. Norum, P. J. Tanner, and T. F. Gallagher, "Rb  $nf$  quantum defects from millimeter-wave spectroscopy of cold  $^{85}\text{Rb}$  Rydberg atoms," *Phys. Rev. A*, vol. 74, Nov. 2006, Art. no. 054502, doi: [10.1103/PhysRevA.74.054502](https://doi.org/10.1103/PhysRevA.74.054502).



**Charles T. Fancher** received the B.S. degree from Worcester Polytechnic Institute, Worcester, MA, USA, in 2010 and the M.S. and Ph.D. degrees from the College of William and Mary, Williamsburg, VA, USA, in 2012 and 2017, respectively, all in physics.

From 2017 to 2019, he was an NRC Postdoctoral Researcher with the Naval Research Laboratory, Washington, DC, USA, where he conducted research on atom interferometry and nanophotonics. His dissertation research included novel

control techniques for ultracold atomic systems. He is currently a Physicist with The MITRE Corporation, McLean, VA, USA, where he is working on atomic and photonic sensors with applications in navigation, imaging, and atmospheric sensing.

Dr. Fancher is also a member of the Optical Society of America and the American Physical Society.



**David R. Scherer** (Senior Member, IEEE) received the B.S. degree in electrical engineering from Boston University, Boston, MA, USA, in 1999, and the M.S. and Ph.D. degrees in optical sciences from the University of Arizona, Tucson, AZ, USA, in 2002 and 2007, respectively.

From 2012 to 2018, he was a Senior Physicist with Microchip, Beverly, MA, USA, where he advanced several efforts related to next-generation atomic clocks, including development of a trapped-ion prototype clock, as well as a demonstration of the world's smallest and lowest-power cold atom system. From 2008 to 2012, he was a Principal Scientist with Physical Sciences Inc. (PSI), Andover, MA, USA, where he led several government-sponsored research projects in the areas of atomic sensors and integrated photonics. He is currently a Lead Scientist with The MITRE Corporation, Bedford, MA, USA, where he is working on novel applications of atomic clocks. His dissertation research focused on interferometry with ultracold atoms. His research interests include applications of atomic clocks, precise timing, and quantum sensors for navigation, communication, and sensing applications.

Dr. Scherer is a Senior Member of the *Optical Society of America* and a member of the Institute of Navigation. He is currently a Committee Member on IEEE Standard 1193, has served on the technical planning committee of the IEEE Frequency Control Symposium, and was the Chair of the Boston Chapter of the IEEE Photonics Society.



**Marc C. St. John** (Member, IEEE) received the B.S. degree in physics from Furman University, Greenville, SC, USA, in 1994 and the M.S. degree in electrical and computer engineering from the Georgia Institute of Technology, Atlanta, GA, USA, in 1996.

He is currently a Principal Engineer with The MITRE Corporation, McLean, VA, USA, where he is working on novel and robust electromagnetic spectrum sensors, advancing software-defined, multifunction wireless systems, and

methods for electromagnetic compatibility between spectrum dependent applications. From 1997 to 2005, he was a Principal Engineer with Hughes Network Systems, where he researched and developed satellite communications electronics.

Dr. St. John was a Member of International Microwave Symposium (IMS) Steering Committee.



**Bonnie L. Schmittberger Marlow** received the A.B. degree from Bryn Mawr College, Bryn Mawr, PA, USA, in 2010 and the A.M. and Ph.D. degrees from Duke University, Durham, NC, USA, in 2013 and 2016, respectively, all in physics.

She is currently a Lead Scientist with The MITRE Corporation, McLean, VA, USA, where she is working on atomic and optical sensors for applications in communications and navigation.

From 2016 to 2018, she was a Postdoctoral Researcher with the Joint Quantum Institute, where she worked with quantum states of light for applications in metrology. Her graduate research focused on nonlinear optics in ultracold atoms.

Dr. Marlow is a Member of the *Optical Society of America*.